Energy-Dependent Kinetic Method: Application to the Multicompetitive Fragmentation Pathways of Protonated Peptides

Isabelle Compagnon and Philippe Dugourd*

Université de Lyon, Université Lyon 1, CNRS, LASIM UMR 5579, 43 Bd du 11 Novembre 1918, 69622 Villeurbanne cedex, France

A variation of the kinetic method for the analysis of fragmentation patterns in mass spectra is proposed. The procedure presents three notable features: no evaluation of the effective temperature of the parent ion is required; the ratio of the activation energies for all competitive channels at play are provided; and the measurement is not biased by the mass discrimination of the instrument. The method is based on the analysis of mass spectra recorded as a function of both the excitation energy and the excitation time. Collision-activated dissociation of protonated Leu−enkephalin achieved in a quadrupolar ion trap and analyzed with this method is presented.

1. Introduction

Gas-phase ion thermochemistry is addressed by a number of techniques based on the dissociation of an activated molecular ion or complex, aiming at providing energy and entropy data. The activation energy of chemical reactions or, reversely, the fragmentation energy of covalent bonds as well as proton, electron, and metal affinities, solvent binding energy, and so forth were thus provided for a vast amount of systems over decades.[1]

The well-established guided ion beam technique consists of monitoring the energy of a single collision between the ion of interest and a neutral target gas in order to measure the energy threshold for the different dissociation channels.[2,3] All kinds of systems have been investigated, although a limitation arises for large molecules as the energy of one single collision becomes insufficient to provoke fragmentation. A similar approach based on surface-induced dissociation of ions may be employed to overcome this limitation.[4,5]

With the rise of ion traps offering long observation time windows, the so-called "slow heating methods" became an alternative of choice.[6] These methods rely on the measurement of the dissociation rate constants rather than energy thresholds. Among them, the blackbody infrared radiation dissociation (BIRD) technique is canonical, as the temperature of the ions is known. In these kinds of experiments, the ions are trapped for seconds in a Fourier transform mass spectrometer under a low pressure and absorb the blackbody radiation emitted by the walls of the vacuum chamber. In such conditions, the ions are in thermal equilibrium with the walls, and the thermochemical data derived this way are absolute.[7,8] BIRD was, in particular, successfully applied to large biomolecules.[9]

In the case of other slow-heating methods, such as IR multiphoton dissociation (IRMPD) or collisional activation (CAD), the temperature of the ions is not defined, and the question of the energy available in the system for fragmentation (often referred to as an effective temperature) has been considerably questioned.[10–14] The case of collisional activation

in a quadrupolar ion trap is of major practical importance since its efficiency, ease-of-use, and facility to implement make it a routine technique in mass spectrometry. Accurate modeling of the temperature is bound to the knowledge of the collision cross section of the ions and the energy transferred during the collisions. Alternatively, calibration based on comparison with the BIRD experiment was proposed.[15] In this context, the kinetic method originally proposed by Cooks[16,17] deserves special attention due to it extensive use in the field of affinity measurements. The kinetic method provides the relative activation energy of two competitive fragmentation channels by means of comparing their rate constants. The effective temperature is evaluated beforehand by calibration with a set of reference molecules. Refinements of the kinetic method, known as the extended kinetic method, were proposed in order to complete the thermochemical description with the entropy data.[18,19]
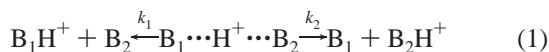
In this article, we propose a variation of the kinetic method based on time- and energy-resolved measurements. The present method consists of recording mass spectra as a function of both the collision energy and the excitation time. The individual rate constant of each fragmentation channel is first obtained as a function of the collision energy. Relative activation energies are then deduced from the evolution of these fragmentation rate constants with the collision energy.

After a summary of the kinetic method in section 2, the alternative procedure proposed in this work (the energy-dependent kinetic method) is presented in section 3. Results obtained on protonated enkephalin are presented in the last section.

2. Kinetic and Extended Kinetic Methods

The kinetic method was first employed for three-body complexes.[16] For example, a loosely bound complex such as the proton-bound dimer $B_1\cdots H^+\cdots B_2$ dissociates along the two major competitive pathways as shown in eq 1. If the proton affinities of B_1 and B_2 are close, both fragments can be observed in the mass spectrum under activation. Other minor fragmentation channels are usually neglected

* To whom correspondence should be addressed. E-mail: dugourd@lasim.univ-lyon1.fr.

$$B_1H^+ + B_2 \underset{k_1}{\leftarrow} B_1 \cdots H^+ \cdots B_2 \underset{k_2}{\rightarrow} B_1 + B_2H^+ \qquad (1)$$

The rates ratio k_1/k_2 is given by the measurement of the ion abundance ratio $[B_1H^+]/[B_2H^+]$ in the mass spectrum.

The simplest relation between the rate constants and the temperature is given by the Arrhenius law in the following equation

$$k_i(T_{eff}) = A_i \exp(-Ea_i/RT_{eff}) \qquad (2)$$

where the preexponential factor A_i accounts for the entropy of activation of the ith dissociation channel, Ea_i is the activation energy of this dissociation, and T_{eff} is the effective temperature of the parent. Although the preexponential factor may vary with temperature, the variation of the exponential term is prominent, and the so-called Arrhenius plot ln $k(T_{eff})$ versus $1/T_{eff}$ is usually strongly linear in the range of temperatures accessible in a given experiment.

The natural logarithm of the rate ratio reads

$$\ln(k_1(T_{eff})/k_2(T_{eff})) = \ln A_1 - \ln A_2 + (Ea_2 - Ea_1)/RT_{eff} \qquad (3)$$

More sophisticated models for the variations of the rate constants with the temperature lead to similar forms.[20,21]

In the standard kinetic method, the entropy terms are assumed to be similar and cancel each other. This assumption applies to complexes where B_1 and B_2 are of similar chemical structure, which leads to eq 4

$$\ln(k_1(T_{eff})/k_2(T_{eff})) = (Ea_2 - Ea_1)/RT_{eff} \qquad (4)$$

To determine the proton affinity of a molecule B_1, a series of $B_1H^+B_2(i)$ complexes is investigated. $B_2(i)$ are molecules for which the proton affinity is known. All of the measurements must be performed under the same conditions, ensuring that T_{eff} is the same for all complexes. The plot of $\ln(k_1/k_2\{i\})$ versus $Ea_2\{i\}$ is linear, with a slope equal to $1/RT_{eff}$. This gives a value for T_{eff}. The proton affinity of B_1 is then directly deduced from eq 4 using the known value of one of the reference molecules.

The extended kinetic method later reduced the errors introduced by the approximation on equivalent entropies by performing measurements at different T_{eff} values.[18,19] By this, the relative activation energies and entropies are obtained from the plot of $\ln(k_1/k_2)$ versus $1/RT_{eff}$, as shown in eq 3. The slope gives the relative activation energy, and the y intercept gives the entropy term.

It should be noted that the measurement is biased if the detection efficiency of the instrument depends on the mass. Indeed, the abundance ratio actually observed in the mass spectra is $\Omega_1[B_1H^+]/\Omega_2[B_2H^+]$, where Ω_1 and Ω_2 are the detection efficiencies for the ions B_1H^+ and B_2H^+, respectively. Hence, the quantity measured is $\ln(\Omega_1/\Omega_2) + \ln(k_1/k_2)$ instead of $\ln(k_1/k_2)$, which leads to a systematic instrumental error.

Despite intrinsic limitations and approximations, the kinetic method is attractive for its simplicity and is probably the most widely used for thermochemical measurements. Consequently, it is also the subject of active discussions and continuous improvements.[21-28]

3. Energy-Dependent Kinetic Method

To our knowledge, the kinetic method has not been employed so far for large molecular ions with complex fragmentation patterns. In the following section, we propose an alternative procedure relevant to such systems, allowing multiple competi-

tive fragmentation channels to be taken into account and avoiding the recourse to a series of reference ions.

Time-Resolved Measurements. In the first place, the individual rate constant of each fragmentation channel is obtained by means of time-resolved measurements. The kinetics of the parent ion M follows a simple exponential decay driven by the total fragmentation rate k_M, as shown in eq 5

$$M(t,T_{eff}) = M(t=0) \exp(-k_M(T_{eff})*t) \qquad (5)$$

The decay of the parent ion yields various fragments B_i with individual rate constants k_i. The total rate constant

$$k_M = \sum_i k_i$$

is the slope of the linear plot of $-\ln(M(t,T_{eff})/M(0,T_{eff}))$ versus time. In an ion trap resonant activation experiment, the trapped ions are selectively excited by a resonant rf field. Due to this additional potential, the selected ions are accelerated and thus undergo collisions of increased energy with the bath gas, which conducts to fragmentation. After fragmentation, the ion has a different mass and is no longer sensitive to the selective excitation. The fragment therefore relaxes by collisions with the bath gas ($\approx 10^4$ collisions/s). In mild excitation conditions, the thermalization of the fragment is expected to be fast enough to prevent secondary fragmentation of the first generation of fragments. Their appearance therefore follows a simple first-order kinetics described by eqs 6 and 7

$$\sum_i B_i(t,T_{eff}) + M(t,T_{eff}) = M(0,T_{eff}) \qquad (6)$$

$$B_i(t,T_{eff}) = \frac{k_i(T_{eff})}{k_M(T_{eff})}(M(0,T_{eff}) - M(t,T_{eff})) \qquad (7)$$

Once the total fragmentation rate k_M is evaluated from eq 5, the individual rates k_i are given by eq 8

$$k_i(T_{eff}) = \frac{B_i(t,T_{eff}) \times k_M(T_{eff})}{M(0,T_{eff}) - M(t,T_{eff})} \qquad (8)$$

Energy-Resolved Measurements. The phenomenological Arrhenius law (eq 2) is used to describe the variations of the rate constants with the effective temperature of the parent ion.

A series of measurements of the rate constants is performed for different values of the excitation energy by changing the amplitude of the rf excitation field. An increase in the excitation energy corresponds to an increase in the effective temperature. Yet, the exact value of the latter remains unknown. One of the fragmentation channels is then chosen as the internal reference. Its rate constant is noted as k_0, whereas the rates of the other competitive channels are noted as k_i. The k_0 and k_i are related to each other by the following relations

$$\ln k_0(T_{eff}) = \ln A_0 - Ea_0/RT_{eff} \qquad (9)$$

$$\ln k_i(T_{eff}) = \ln A_i - Ea_i/RT_{eff} = \ln A_i -$$
$$Ea_i/Ea_0*Ea_0/RT_{eff} \qquad (10)$$

$$= \ln A_i - Ea_i/Ea_0*\ln A_0 + Ea_i/Ea_0*\ln k_0(T_{eff})$$

The $\ln k_i(T_{eff})$ is then plotted versus $\ln k_0(T_{eff})$ for each fragmentation channel. According to eq 10, the slope of the

Fragmentation Pathways of Protonated Peptides

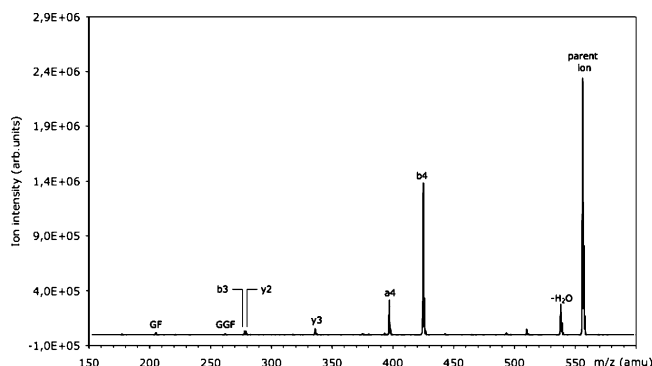*J. Phys. Chem. A, Vol. 111, No. 42, 2007* **10637**

Figure 1. Mass spectrum of protonated Leu−enkephalin under collisional activation (with an excitation time = 10 ms and a rf excitation amplitude = 0.590 V).
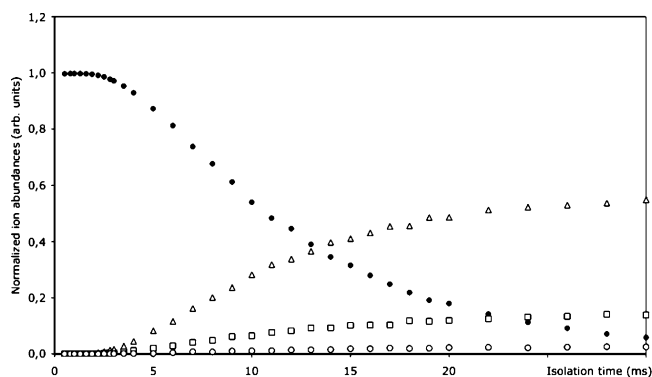

Figure 2. Normalized abundances of the parent ion (filled circles), loss of water (open squares), the b4 fragment (open triangles), and the y3 fragment (open circles) as a function of excitation time for the rf excitation amplitude = 0.590 V. Other fragments are not shown for clarity.
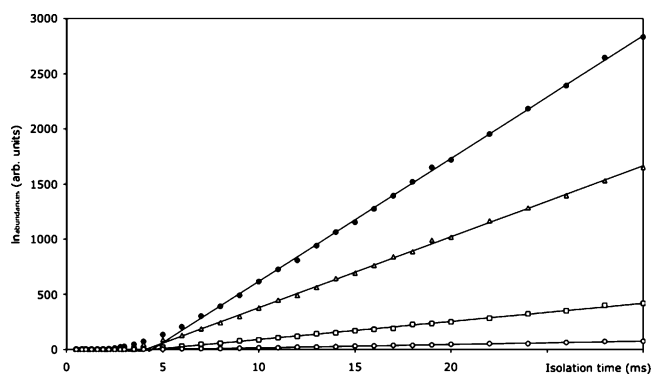

Figure 3. Kinetic plot of the parent ion (filled circles) (eq 12), loss of water (open squares), the b4 fragment (open triangles), and the y3 fragment (open circles) (eq 13) as a function of excitation time for a rf excitation amplitude = 0.590 V.

plot directly provides the relative activation energy Ea_i/Ea_0 for a given fragment. The entropy term can be obtained from the y intercept.

Mass Discrimination. If the measurements of ion abundances are biased by the detection efficiency Ω of the instrument, the rate constants measured are slightly erroneous, and eq 10 is modified as follow

$$\ln(\Omega_i k_i) = \ln(\Omega_i A_i) - Ea_i/Ea_0*\ln(\Omega_0 A_0) + Ea_i/Ea_0*\ln(\Omega_0 k_0) \quad (11)$$

The y intercept is effected by the instrumental error, but the slope is unchanged; therefore, the mass discrimination does not influence the measurement of the relative activation energies.
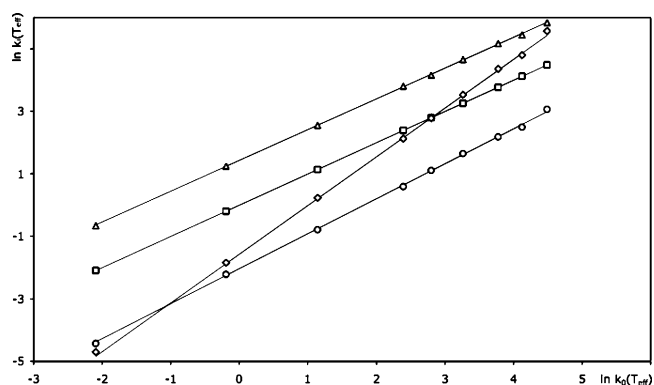

Figure 4. Rate constants corresponding to the b4 fragment (open triangles), loss of water (open squares), the y3 fragment (open circles), and the a4 fragment (open diamonds) plotted as a function of the rate constant corresponding to the loss of water.

Finally, the energy-dependent kinetic method extends the application field of the kinetic method to large systems with multiple competitive fragmentation channels. In contrast to other kinetic methods, the evaluation of T_{eff} is not used to determine relative activation energies. This removes a source of uncertainty and avoids the need for a series of reference systems. The latter point would indeed become an issue for large molecular ions as the collision cross sections and energy conversion efficiencies may strongly vary, thus forbidding the temperature to be assumed as a constant for a series of molecules. The activation energies measured for all fragmentation channels are relative to one specific channel chosen as the internal reference and are not effected by the mass discrimination. These improvements are obtained at the cost of both time- and energy-resolved measurements, which compares to the cost of the extended kinetic method, where temperature-dependent measurements are performed for a series of reference systems.

4. Experimental Section

The protonated peptide ions were formed by electrospray ionization (ESI) and trapped and dissociated by collisional activation (CAD) in a quadrupolar ion trap mass spectrometer (LCQ duo, ThermoElectron). Leu−enkephalin was purchased from Sigma and dissolved at a concentration of 500 μM in H_2O/CH_3OH 1:1 (v/v) with 1% of acetic acid. The solution was electrosprayed, and the parent ion was isolated at mass 556.6 and then excited with a resonant rf excitation field to fragment by collisions with the buffer gas (He, 10^{-2} Torr). The mass spectra were averaged over 90 scans, and the abundance of the parent ion and each fragment was monitored as a function of excitation time (ranging from 0.5 to 600 ms) and for various excitation energies (amplitude of the rf resonant excitation field ranging from 400 to 750 mV), which corresponds to increasing temperatures.

Analysis of the Protonated Enkephalin Fragmentation Patterns. A mass spectrum is presented in Figure 1. The typical loss of water and the b fragment usually observed for protonated peptides under collisional activation are featured. A smaller amount of fragments a and y and internal fragments GF and GFF are also observed.

In each mass spectrum, the abundances of the parent and the fragments ions are normalized to the initial abundance of the parent ion. They are plotted as a function of isolation time for a given excitation energy, as shown in Figure 2. An induction period of a few milliseconds is necessary to elevate the temperature of the parent ion prior to dissociation, as reported in refs 15 and 29. Then, the parent ion abundance undergoes

TABLE 1: Dissociation Rates[a]

ion	(m/z)	rf excitation amplitude (V)								
		0.426	0.473	0.521	0.568	0.593	0.618	0.627	0.710	0.758
parent	(556.3)	0.673 ± 0.009	4.75 ± 0.02	18.7 ± 0.2	72.7 ± 0.9	111.4 ± 0.7	196 ± 2	364 ± 6	517 ± 15	922 ± 21
Fragments										
H$_2$O loss	(538.3)	0.123 ± 0.003	0.82 ± 0.01	3.12 ± 0.04	10.9 ± 0.2	16.40 ± 0.3	26.07 ± 0.7	43.5 ± 0.8	62 ± 2	89 ± 3
b4	(425.2)	0.517 ± 0.007	3.49 ± 0.02	12.8 ± 0.1	45.0 ± 0.7	64.3 ± 0.5	106 ± 1	177 ± 2	232 ± 5	345 ± 5
a4	(397.2)	0.009 ± 0.001	0.159 ± 0.004	1.27 ± 0.04	8.4 ± 1	16.1 ± 0.3	35 ± 1	78 ± 3	122 ± 7	264 ± 10
y3	(336.2)	0.0119 ± 0.0009	0.109 ± 0.003	0.45 ± 0.02	1.80 ± 0.07	3.02 ± 0.07	5.3 ± 0.3	8.9 ± 0.4	12 ± 1	21 ± 1
b3	(278.1)	0.0020 ± 0.0004	0.016 ± 0.002	0.093 ± 0.008	0.50 ± 0.05	0.94 ± 0.04	2.1 ± 0.1	5.2 ± 0.4	9.3 ± 0.7	28 ± 3
y2	(279.2)	0.0046 ± 0.0006	0.048 ± 0.002	0.21 ± 0.01	0.88 ± 0.04	1.42 ± 0.08	2.4 ± 0.1	4.9 ± 0.4	7.8 ± 0.6	16 ± 2
GF	(205.1)		0.013 ± 0.002	0.090 ± 0.008	0.50 ± 0.04	0.97 ± 0.8	1.8 ± 0.2	4.4 ± 0.5	6.1 ± 0.4	13 ± 1
GGF	(262.1)		0.0027 ± 0.0007	0.028 ± 0.005	0.23 ± 0.02	0.43 ± 0.03	1.09 ± 0.09	2.2 ± 0.3	4.8 ± 0.5	9.2 ± 0.8

[a] The dissociation rates (s^{-1}) were measured for different RF excitation amplitudes. The uncertainties are given for a confidence of 76%.

an exponential decay, while the fragment ion appearances follow simple monoexponential kinetics described by eq 7. The conservation of the total number of ions in the trap (eq 6) is verified experimentally. To determine the decay rates, the curves shown in Figure 2 are replotted in Figure 3 with a log scale, using the following procedure.

The decay rate k_M for the parent ion is derived by plotting

$$k_M*t = -\ln(M(t,T_{eff})/M(0,T_{eff})) \qquad (12)$$

versus time. The individual rate k_i of each fragment is given by eq 8. In order to allow a straightforward evaluation of the statistical error, the value of k_M is not directly introduced in eq 8. Rather, each individual rate is derived from the original set of data {$B_i(t,T_{eff})$; $M(t,T_{eff})$; $M(0,T_{eff})$} by plotting

$$k_i*t = B_i(t,T_{eff}) \times \frac{\ln(M(t,T_{eff})/M(0,T_{eff}))}{M(t,T_{eff}) - M(0,T_{eff})} \qquad (13)$$

versus time. The plots obtained for the parent and three different fragments are shown in Figure 3. After exclusion of the induction period, a linear behavior is observed. The rates corresponding to the appearance of each fragment and the disappearance of the parent are obtained by the slope of the linear adjustment of the data shown in Figure 3. The kinetic plots shown in Figure 3 are linear for both the parent and the fragments, which validates the simple kinetic model employed (eqs 5 and 7).

The same analysis was performed for a set of rf excitation amplitudes, which correspond to different (unknown) temperatures. The resulting rates are reported in Table 1. The total fragmentation rate of protonated enkephalin ranges from 0.67 to 922 s^{-1}. Comparison with temperature-resolved experiments[29] shows that this corresponds to effective temperatures ranging from 500 to 700 K.

The loss of water is chosen for reference. Its rate constant is noted as $k_0(T_{eff})$, and its activation energy is Ea_0. The data shown in Table 1 are reported on a graph; $\ln k_i(T_{eff})$ is plotted versus $\ln k_0(T_{eff})$. The results are shown in Figure 4. For each fragment, a linear plot is observed. According to eq 10, the slope of the linear adjustment is equal to Ea_i/Ea_0. The relative activation

TABLE 2: Relative Fragmentation Energies for the Different Fragmentation Channels of Protonated Enkephalin[a]

	from this work	statistical error	from ref 30
H$_2$O loss	1	reference	1
b4	0.984	0.002	0.95
a4	1.559	0.007	1.08
y3	1.118	0.008	}1.14
y2	1.16	0.02	
b3	1.48	0.02	1.18
GF	1.46	0.02	}1.25
GFF	1.72	0.03	

[a] The uncertainties are given for a confidence of 76%.

energies of all of the competitive fragmentation channels are thus measured with reference to the loss of water and reported in Table 2

Results. The activation energies for the two main channels, which correspond to the loss of water and b4, are extremely close. This is in agreement with the conclusions of Williams et al. who obtained values undistinguishable within the error bars for these two channels[29] (0.99 ± 0.07 and 1.11 ± 0.09 eV, respectively).

Results of RRKM simulations for the primary fragmentation channels of enkephalin from ref 30 are reported in Table 2 as well. Our findings are in qualitative agreement with these predictions. The H$_2$O and b4 channels are also found to be very close in energy, b4 being the lowest, which again matches our conclusions. In our work and in ref 30, the b3 fragment shows a higher activation energy than that of b4, which is consistent with the typical behavior of nonbasic peptides.[31] It is also observed that $Ea(a4) > Ea(b4)$, although our measurements lead to a higher gap than predicted. An excellent quantitative agreement is observed for the y fragments (treated at once in the simulations). Finally, the internal fragments (also treated at once in the simulations) show high activation energy in both works, though the experimental values are significantly higher than the calculated ones.

Uncertainties. The errors bars on the relative energies reported in Table 2 are very small. As compared to the classical kinetic method, we obtained the rate constants by the mean of time-resolved measurements (15−20 mass spectra) instead of one single rate ratio measurement. The kinetic plots (Figure 3)

are strongly linear and provide accurate rate constants. The time-resolved measurements were reproduced for nine different temperatures. The linearity of the Arrhenius plots (Figure 4) is also verified, and the statistical error on the slope is very small. Therefore, the large number of spectra explains the very small error bars reported in Table 2.

Nevertheless, the meaning of the error bars must be discussed since two major approximations of the kinetic method remain. First, the kinetic plots are based on the description of a single generation of fragments, which is still a matter of debate.[32,33] Second, no systematic error due to the use of the Arrhenius law was taken into account.

Note that the choice of one internal reference among all competitive fragments removes a source of error of other kinetic methods, as the temperature does not need to be derived from external references. The systematic error due to mass discrimination is also avoided.

5. Conclusion

We have proposed a variation of the kinetic method based on time- and energy-resolved measurements. In contrast to other kinetic methods, the effective temperature of the system undergoing fragmentation is not evaluated. In addition, the relative activation energies are obtained with a very good statistical accuracy. Still, some restrictive features of the kinetic methods must be regarded; the resulting activation energies are not absolute and are bound to the model used for the dependence of the rate constants with the temperatures (here, we have used the common Arrhenius law).

Besides the temperature issue and the gain in accuracy, the main advantage of the present procedure is to extend the use of kinetic methods to large molecules with complex fragmentation patterns. We have presented the analysis of the fragmentation of protonated Leu−enkephalin by collision-induced dissociation in a quadrupolar ion trap. The relative activation energies measured for the different competitive fragmentation channels are in good agreement with the literature.

References and Notes

(1) Ervin, K. M. *Chem. Rev.* **2001**, *101*, 391−444.
(2) Armentrout, P. B. *Int. J. Mass Spectrom.* **2000**, *200*, 219−241.
(3) Armentrout, P. B. *J. Am. Soc. Mass Spectrom.* **2002**, *13*, 419−434.
(4) Dongre, A. R.; Somogyi, A.; Wysocki, V. H. *J. Mass Spectrom.* **1996**, *31*, 339−350.
(5) Mabud, M. D. A.; Dekrey, M. J.; Cooks, R. G. *Int. J. Mass Spectrom. Ion Processes* **1985**, *67*, 285−294.
(6) McLuckey, S. A; Goeringer, D. E. *J. Mass Spectrom.* **1997**, *32*, 461−474.
(7) Dunbar, R. C. *Mass Spectrom. Rev.* **2004**, *23*, 127−158.
(8) Dunbar, R. C.; McMahon, T. B. *Science* **1998**, *279*, 194−197.
(9) Price, W. D.; Schnier, P. D.; Williams, E. R. *Anal. Chem.* **1996**, *68*, 859−866.
(10) Ervin, K. M. *Int. J. Mass Spectrom.* **2000**, *196*, 271−284.
(11) Schnier, P. D.; Jurchen, J. C.; Williams, E. R. *J. Phys. Chem. B* **1999**, *103*, 737−745.
(12) Goeringer, D. E.; McLuckey, S. A. *J. Chem. Phys.* **1996**, *104*, 2214−2221.
(13) Tolmachev, A. V.; Vilkov, A. N.; Bogdanov, B.; Pasa-Tolic, L.; Masselon, C. D.; Smith, R. D. *J. Am. Soc. Mass Spectrom.* **2004**, *15*, 1616−1628.
(14) Plass, W. R.; Cooks, R. G. *J. Am. Soc. Mass Spectrom.* **2003**, *14*, 1348−1359.
(15) Asano, K. G.; Butcher, D. J.; Goeringer, D. E.; McLuckey, S. A. *J. Mass Spectrom.* **1999**, *34*, 691−698.
(16) McLuckey, S. A.; Cameron, D.; Cooks, R. G. *J. Am. Chem. Soc.* **1981**, *103*, 1313−1317.
(17) Cooks, R. G.; Wong, P. S. H. *Acc. Chem. Res.* **1998**, *31*, 379−386.
(18) Cheng, X. H.; Wu, Z. C.; Fenselau, C. *J. Am. Chem. Soc.* **1993**, *115*, 4844−4848.
(19) Cerda, B. A.; Wesdemiotis, C. *J. Am. Chem. Soc* **1996**, *118*, 11884−11892.
(20) Fernandez-Ramos, A.; Miller, J. A.; Klippenstein, S. J.; Truhlar, D. G. *Chem. Rev.* **2006**, *106*, 4518−4584.
(21) Laskin, J.; Futrell, J. H. *J. Phys. Chem. A* **2000**, *104*, 8829−8837.
(22) Ervin, K. M. *Int. J. Mass Spectrom.* **2000**, *196*, 271−284.
(23) Ervin, K. M.; Armentrout, P. B. *J. Mass Spectrom.* **2004**, *39*, 1004−1015.
(24) Ervin, K. M. *J. Am. Soc. Mass Spectrom.* **2002**, *13*, 435−452.
(25) Armentrout, P. B. *J. Am. Soc. Mass Spectrom.* **2000**, *11*, 371−379.
(26) Bouchoux, G.; Sablier, M.; Berruyer-Penaud, F. *J. Mass Spectrom.* **2004**, *39*, 986−997.
(27) Wesdemiotis, C. *J. Mass Spectrom.* **2004**, *39*, 998−1003.
(28) Laszlo, D.; Vékey, K. *J. Mass. Spectrom.* **2003**, *38*, 1025−1042.
(29) Schnier, P. D.; Price, W. D.; Strittmatter, E. F.; Williams, E. R. *J. Am. Soc. Mass Spectrom.* **1997**, *8*, 771−780.
(30) Laskin, J. *J. Phys. Chem. A* **2006**, *110*, 8554−8562.
(31) Paizs, B.; Suhai, S. *J. Am. Soc. Mass Spectrom.* **2004**, *15*, 103−113.
(32) Black, D. M.; Payne, A. H.; Glish, G. L. *J. Am. Soc. Mass Spectrom.* **2006**, *17*, 932−938.
(33) Rakov, V. S.; Borisov, O. V.; Whitehouse, C. M. *J. Am. Soc. Mass Spectrom.* **2004**, *15*, 1794−1809.